A tumor suppressor role of the Bub3 spindle checkpoint protein after apoptosis inhibition

Sara Morais da Silva,[1] Tatiana Moutinho-Santos,[1] and Claudio E. Sunkel[1,2]

[1]Instituto de Biologia Molecular e Celular and [2]Instituto de Ciências Biomédicas de Abel Salazar, Universidade do Porto, 4099 Porto, Portugal

Most solid tumors contain aneuploid cells, indicating that the mitotic checkpoint is permissive to the proliferation of chromosomally aberrant cells. However, mutated or altered expression of mitotic checkpoint genes accounts for a minor proportion of human tumors. We describe a *Drosophila melanogaster* tumorigenesis model derived from knocking down spindle assembly checkpoint (SAC) genes and preventing apoptosis in wing imaginal discs. *Bub3*-deficient tumors that were also deficient in apoptosis displayed neoplastic growth, chromosomal aneuploidy, and high proliferative potential after transplantation into adult flies. Inducing aneuploidy by knocking down CENP-E and preventing apoptosis does not induce tumorigenesis, indicating that aneuploidy is not sufficient for hyperplasia. In this system, the aneuploidy caused by a deficient SAC is not driving tumorigenesis because preventing Bub3 from binding to the kinetochore does not cause hyperproliferation. Our data suggest that Bub3 has a nonkinetochore-dependent function that is consistent with its role as a tumor suppressor.

Introduction

During cellular proliferation, failure of the proper execution or regulation of mechanisms of DNA repair or cell cycle checkpoints will lead to either genomic or chromosomal instability (CIN). During mitosis, failure to correctly segregate sister chromatids results in CIN, which is frequently observed in tumors, and it has been argued to be the primary cause and driving force of tumorigenesis. However, most tumors in addition to aneuploidy have acquired mutations in oncogenes and tumor suppressor genes (Weaver and Cleveland, 2006). The reasons for aneuploidy being the most commonly observed genetic alteration in many types of tumors remain unknown. The spindle assembly checkpoint (SAC) proteins monitor the mitotic transition from metaphase to anaphase, preventing aneuploidy. SAC proteins signal the cell via unattached kinetochores, allowing the progression of mitosis only when the microtubule–kinetochore attachment process is complete. Unattached kinetochores produce a diffusible signal to delay anaphase. This signal works by blocking ubiquitination of cyclin B and Securin by the anaphase-promoting complex/cyclosome (APC/C). APC/C activation is dependent on Cdc20, which in turn is a target of this inhibitory signal (Musacchio, 2011). Several checkpoint proteins

have now been identified, but how they orchestrate communication between local spindle attachment and global cytoplasmic signaling to delay segregation is not thoroughly understood. The existence of conflicting data about the role of checkpoint genes in neoplasia and tumor progression therefore requires further studies in an in vivo situation.

We describe a *Drosophila melanogaster* tumorigenesis model derived from knocking down SAC genes. *Bub3*-deficient tumors display neoplastic growth, widespread chromosomal aneuploidy, and high proliferative potential after transplantation into adult flies. In this system, the aneuploidy caused by a deficient SAC is not the driving force for tumorigenesis because preventing Bub3 from binding to the kinetochore does not cause hyperproliferation. Instead, the removal of the cytosolic pool of Bub3 is essential for transformation to occur. Depletion of the SAC proteins BubR1 and Mad2 also drive tumorigenesis in our system. We propose a new role for the SAC proteins as tumor suppressors.
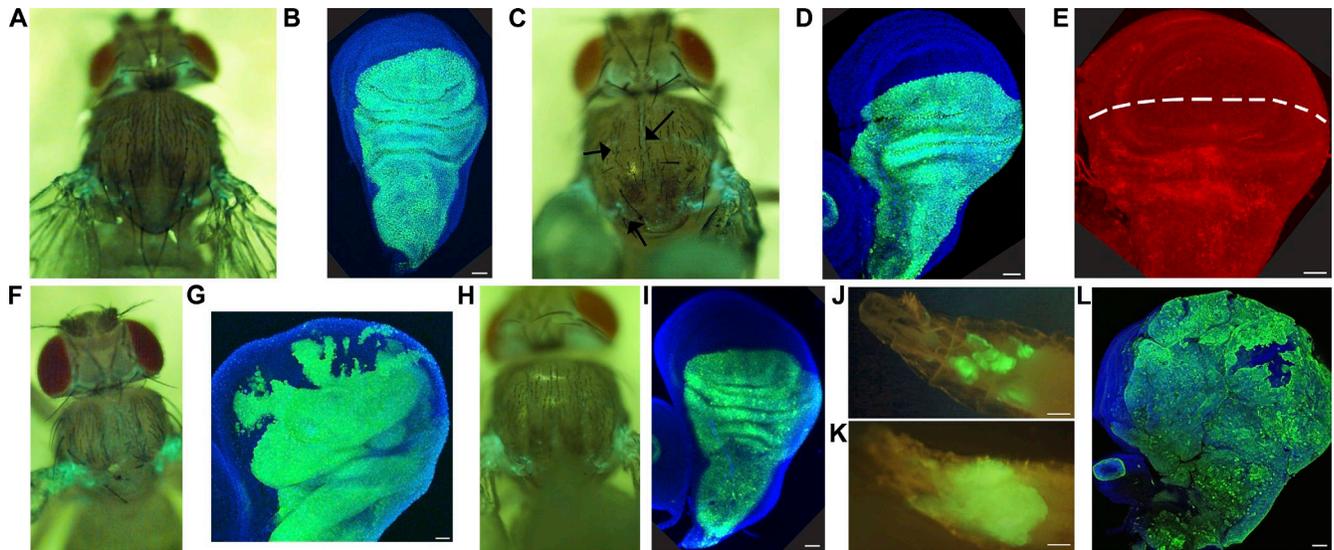
Results and discussion

We addressed the role of checkpoint genes in vivo in *Drosophila*. We knocked down the SAC protein Bub3 (Lopes et al., 2005)

The Rockefeller University Press $30.00
J. Cell Biol. Vol. 201 No. 3 385–393
www.jcb.org/cgi/doi/10.1083/jcb.201210018

JCB 385

Figure 1. **Knockdown of *Bub3* promotes tumorigenesis in *Drosophila* wing discs.** (A and B) GFP expression in the adult (A) and wing disc (B). (C and D) *Bub3* RNAi and GFP expression. Adult thorax (C) showing empty sockets and loss of bristles (arrows) and wing disc (D). Note that the wing disc is smaller than a wt disc. (E) Apoptosis in wing discs expressing *Bub3* RNAi in the dorsal compartment. The dotted line separates the dorsal (bottom) from the ventral (top) sides of the wing disc. (F and G) Coexpression of *Bub3* RNAi, DIAP1, and GFP in the adult thorax (F) and wing disc (G). (H and I) Expression of *Bub3* RNAi, *Drosophila* p53R155H, and GFP. Adult thorax (H) and wing disc (I) showing a similar phenotype to A and B. (J and K) Larvae expressing GFP (top) and expressing *Bub3* RNAi, p35, and GFP (bottom). (L) Wing disc dissected out of an L3 larvae expressing *Bub3* RNAi, p35, and GFP. Note the hyperplasia. Transgenes in this study were driven by the *apterous* promoter. Bars: (B) 70 µm; (D, E, G, and I) 40 µm; (J) 100 µm; (K) 150 µm; (L) 80 µm.

from the dorsal compartment of the wing imaginal disc, leaving the ventral compartment as wild type (wt). As a result, thoraxes of adult flies showed loss of bristles and empty sockets and the wing discs were smaller than wt, showing widespread apoptosis in the dorsal domain (Fig. 1, A–E) that is not observed in wt wing discs (Fig. S2 A). The observed apoptosis was in agreement with the phenotype of the null *Bub3* knockout mouse model (Kalitsis et al., 2000) and the *Drosophila* mutant (Lopes et al., 2005). Interestingly, null mutant mouse embryos for other SAC proteins, such as BubR1 and Mad2, share similar phenotypes (Dobles et al., 2000; Wang et al., 2004). Quantification of the Bub3 depletion revealed that the levels of Bub3 protein were reduced specifically in the dorsal region of the wing disc (Fig. S1, A–C and N). In addition, RNAi knockdown of *Bub3* in the dorsal region of the wing discs prevented the accumulation of mitotic cells after treatment with colchicine, which demonstrates its importance in the SAC response. (Fig. S1, D and M). As compelling evidence indicates that oncogenic changes can prevent apoptosis (Cotter, 2009), we decided to block apoptosis to investigate whether cells would become transformed. When the apoptotic inhibitor DIAP1 (Orme and Meier, 2009) was selectively coexpressed with *Bub3* RNAi in the dorsal compartment of the wing disc, the mutant adult thorax and the wing discs were bigger than in wt, and cellular invasion from one compartment to another was observed (Fig. 1, F and G). Coexpression of the dominant-negative form of p53R155H (Ollmann et al., 2000), and *Bub3* RNAi did not suppress the *Bub3* knocked down apoptotic phenotype, indicating that it does not depend on p53. The same result was obtained with the p53H159N dominant-negative form of the p53 protein (Fig. 1, H and I; and not depicted; Ollmann et al., 2000). Expressing the strong apoptotic inhibitor p35 (Hay et al., 1994) together with *Bub3* RNAi

in the dorsal compartment led to tissue hyperplasia, producing larva with giant wing discs, which fail to pupariate and had a prolonged larval life, during which they grew significantly in size (Fig. 1, J–L). Karyotypic analysis indicated a high degree of aneuploidies that result from disruption of the SAC (Fig. 2, A–C; and for a more comprehensive data on aneuploidies see Table 1). Cellular DNA content analysis by flow cytometry confirmed that the aneuploidy is specific of the cells in which *Bub3* was knocked down (Fig. 2, E, F, H, and I). In addition, the hyperplastic growth was cell autonomous, as the dorsal compartment grew much more than the ventral one (Fig. 2, D and G), indicating that the growth was not the result of compensatory proliferation (Pérez-Garijo et al., 2005). Furthermore, when fragments of hyperplastic discs were transplanted into the abdominal cavity of adult female wt recipients to assay their proliferative potential, they grew, filling the whole abdominal cavity over a relatively short period of time (27 d; Fig. 2 J). Implanted wing discs with *Bub3* knocked down did not grow, and a low percentage of imaginal discs expressing p35 were alive after the test period, but proliferation was very limited, reflecting the relatively low neoplastic capacity of caspase-inhibited apoptotic cells (Pérez-Garijo et al., 2005).

As aneuploidy has been proposed to drive tumor progression (Weaver and Cleveland, 2006), we investigated whether this model of tumorigenesis was a direct consequence of CIN generated by an impaired SAC. Precise interactions between kinetochores and microtubules of the mitotic spindle require CENP-E, a cell cycle–regulated kinesin motor protein (Brown et al., 1994). Cells and mice with reduced CENP-E generate high rates of aneuploidy in the absence of other observable defects (Weaver et al., 2007). When CENP-E was knocked down in the dorsal compartment of the wing disc, adult thoraxes
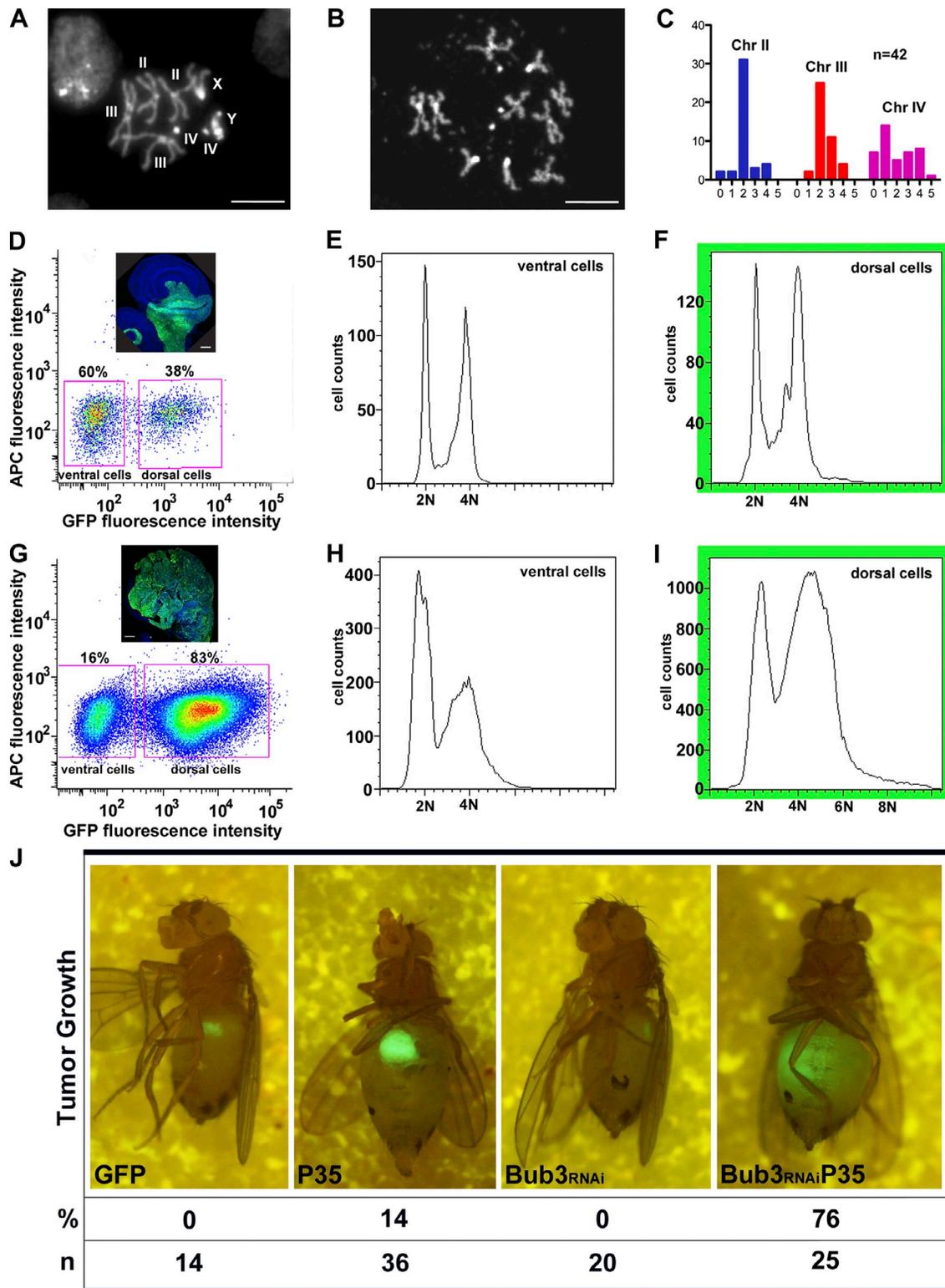
Figure 2. **Bub3 knockdown induces aneuploidy and hyperplasia.** (A–C) Karyotypic analysis of the hyperplastic wing discs expressing Bub3 RNAi, p35, and GFP. (A) wt mitotic cell karyotype where chromosomes I, II, II, and IV as well as the X and Y are shown. (B) Mitotic cell karyotype displaying aneuploidy. (C) Somatic chromosome (Chr) representation of aneuploidies found in hyperplastic wing discs (42 aneuploidies from a total of 63 metaphasic cells counted from three wing discs). (D–I) FACS analysis of dissociated ventral cells (E and H) and dorsal cells (F and I) from wing discs expressing *Bub3* RNAi and GFP (D–F) and from wing discs expressing *Bub3* RNAi, p35, and GFP (G–I). Note the increased number of aneuploid cells in I when compared with H and the higher percentage of GFP cells in the hyperplastic discs (83%; G) when compared with wing discs expressing *Bub3* RNAi (38%; D). The data shown are from a single representative experiment out of three repeats (D–I). (J) Hyperplastic discs were transplanted into adult female hosts to assess their proliferative potential. Discs expressing GFP, GFP and p35, GFP and *Bub3* RNAi, GFP and *Bub3* RNAi, and p35 were implanted; the number of implants and the percentage of discs that grew are shown. Note that the implants grew extensively in the *Bub3* RNAi p35 discs invading the host abdomen. Bars: (A and B) 5 µm; (D) 40 µm; (G) 80 µm.

Table 1. **Aneuploidy in wing imaginal discs**

Genotype (four discs)	Total mitotic cells	Aneuploid cells	Aneuploidy (SD)
			%
Ap-GAL4 UASGFP	653	32	7.75 (0.40)
Ap-GAL4 UASGFP/UASp35	645	75	12.04 (2.51)
Ap-GAL4 UAS*bubR1*RNAi UASGFP/UASp35	415	51	12.43 (1.23)
Ap-GAL4 UAS*mad2*RNAi UASGFP/UASp35	310	35	12.02 (3.38)
Ap-GAL4 UAS*cenpE*RNAi UASGFP/UASp35	1,124	143	12.53 (2.38)
Ap-GAL4 UAS*nsl1*RNAi UASGFP/UASp35	441	81	18.39 (0.63)
Ap-GAL4 UAS*bub3*RNAi UASGFP/UASp35	308	83	27.21 (3.58)
Ap-GAL4 UAS*nsl1*RNAi UASGFP/UAS*bub3*RNAi UASp35	574	195	33.92 (5.36)

showed a reduced number of bristles, and the discs were smaller (Fig. 3, A and B). As a result of RNAi expression, CENP-E protein levels were reduced in the dorsal compartment (Fig. 3 E and Fig. S1 N), and there was apoptosis (Fig. 3 c). Knockdown of CENP-E does not impair SAC signaling, as cells from the dorsal and ventral domains respond equally to colchicine treatment, as the mitotic index remains similar between the two compartments (Fig. 3 D and Fig. S1 M). Blocking apoptosis induced tissue disorganization but did not induce strong hyperplasia, indicating that in this system, tumorigenesis was not being induced by CIN per se (Fig. 3 H). Cellular DNA content analysis by flow cytometry confirmed that a small percentage of CENP-E–depleted cells had aneuploidies (Fig. 3, J, K, M, and N). However, both compartments grew to the same extent, as the cell population maintained a similar proportion of GFP versus non-GFP cells (Fig. 3, I and L). The resulting wing discs were smaller in size when compared with discs in which *Bub3* was knocked down together with expression of p35 (Fig. 3 O). Importantly, in allograph assays (Fig. 3 P), wing discs in which CENP-E was knocked down together with p35 expression grew to the same extent (∼13–14%) as control discs expressing only p35 (Fig. 2 J), confirming that aneuploidy is not sufficient to drive uncontrolled growth. This contrasts with the *Bub3*RNAi/p35 allografts that showed 76% tumor growth. Interestingly, CENP-E knocked down implants failed to grow in these assays (Fig. 3 P).

Bub3 protein is found at unattached kinetochores during prometaphase (Taylor et al., 1998), in inhibitory complexes such as the mitotic checkpoint complex (Sudakin et al., 2001), and in the cytosol of interphase cells (Yoon et al., 2004). We asked whether it was the absence of SAC signaling provided by the kinetochore that promoted hyperplasia or whether it was the absence of the Bub3 cytoplasmic pool that allowed hyperplasia to occur. To prevent kinetochore targeting of Bub3, Nsl1 was depleted. Nsl1 is a protein that resides in the inner plate of the kinetochore and, together with Mis12, forms the Mis12 complex. Nsl1 is required for the assembly and localization of outer kinetochore components, such as the Ndc80 complex (Venkei et al., 2011). We generated a transgenic *Drosophila* expressing Nsl1 RNAi in the dorsal compartment of the wing disc (Fig. 4, A and B). The adult thorax presented multiple empty sockets and missing bristles, and the wing discs were smaller than wt. In addition, SAC signaling was impaired, as there was a decreased mitotic index in the dorsal when compared with

the ventral compartment of wing discs treated with colchicine (Fig. 4 C and Fig. S1 M). We assessed whether the SAC proteins were able to bind kinetochores from Nsl1-depleted cells (Fig. 4, E–X). Immunofluorescence confirmed that Bub3 (Fig. 4, M–P), BubR1 (Fig. 4, Q–T), and Mad1 (Fig. 4, U–X) were not localized at the kinetochores of mitotic dorsal cells in which Nsl1 was depleted. These findings suggest that the SAC was impaired in this system and confirmed that the depletion of Nsl1 prevented Bub3, BubR1, and Mad1 from binding the kinetochore and generating the SAC signal. Depletion of Nsl1 caused apoptosis in dorsal cells (Fig. 4 D), and it was inhibited by expression of p35, but no hyperplasia or tissue disorganization was observed (Fig. 4 Y). These results indicated that preventing Bub3, BubR1, and Mad1 from binding the kinetochore and therefore impairing SAC signaling was not sufficient to cause the overgrowth. Next, we depleted Nsl1 and Bub3 to remove the ability of SAC proteins to signal from the kinetochore and to remove cytosolic Bub3. Simultaneous knockdown of Nsl1 and *Bub3* and apoptosis inhibition by expression of p35 resulted in hyperplasia at efficiencies equivalent to discs expressing *Bub3* RNAi and p35 (Fig. 4 Z). Knocking out SAC did not increase frequency of hyperplasia resulting from *Bub3* RNAi and p35 expression. Interestingly, although the aneuploidy is not the driving force in these overgrowths, this genotype together with the one in which only *Bub3* is knocked down in the presence of p35 reveals the highest percentage of aneuploidies (Table 1). Allograph experiments with wing discs having *Bub3* and Nsl1 knocked down and expressing p35 revealed that they overgrew by filling the abdominal cavity of the female host, whereas discs knocked down for either Nsl1 or Nsl1 and p35 failed to grow (Fig. 4 A′). Collectively, these results suggested a tumor suppressor role for Bub3.

We asked whether other SAC proteins could also promote tumorigenesis. Accordingly, *BubR1* and *Mad2* were knocked down specifically from the dorsal compartment of the wing disc (Fig. 5, A and D). Apoptosis was observed in cells in which either *BubR1* or *Mad2* were depleted (Fig. 5, B and E). Interestingly, wing imaginal discs from *Mad2*[P] homozygotes flies (Buffin et al., 2007) also showed significant levels of apoptosis (Fig. S2, C and D). In addition, when apoptosis was blocked by coexpressing p35, tumorigenesis occurred (Fig. 5, C and F). Tumorigenesis was induced by the absence of any of the three SAC proteins Bub3, BubR1, and Mad2, but they do so at different rates. Although, for the depletion of the Bub3 protein, we obtained hyperplastic wing discs in 100% of third instar
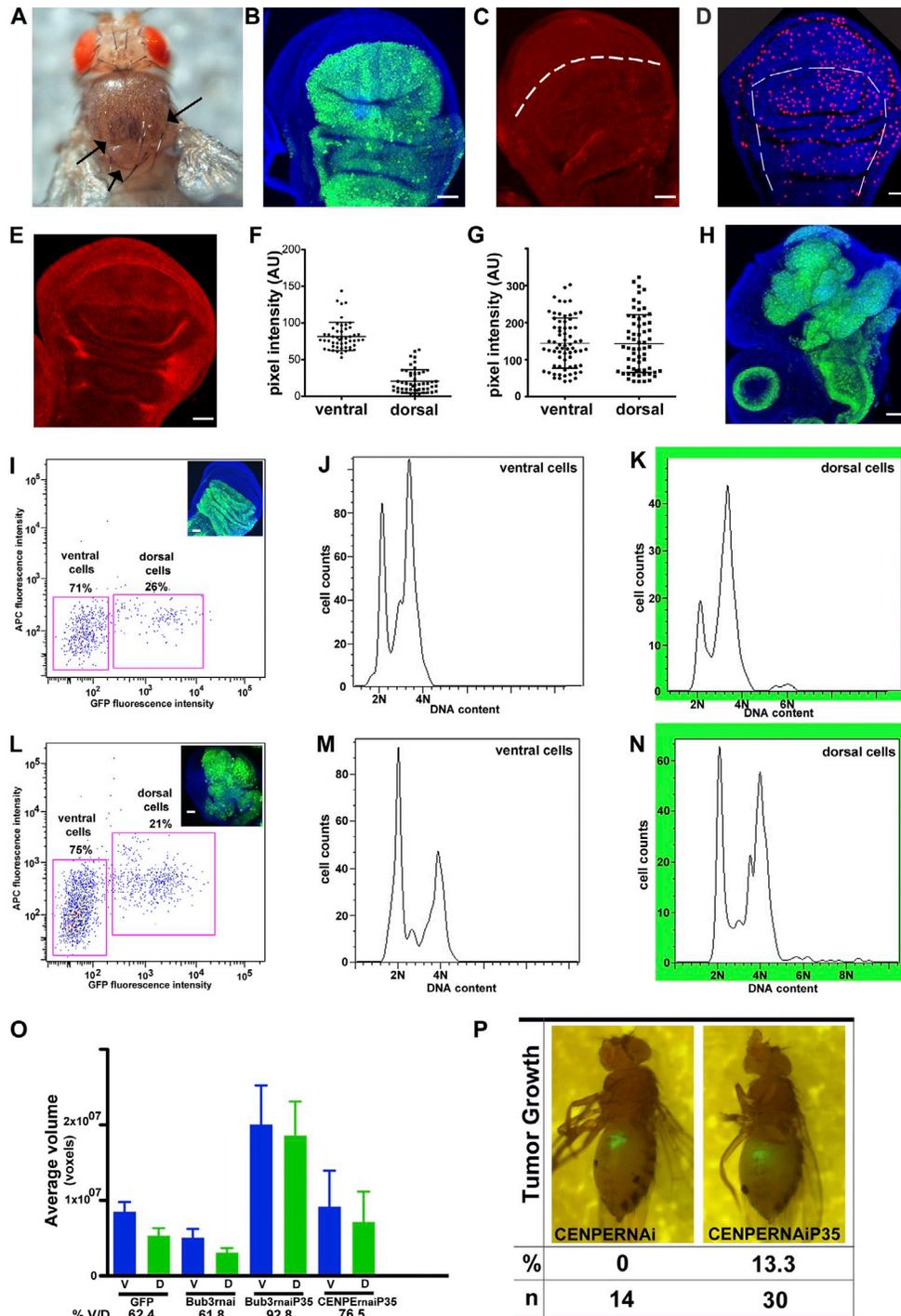
Figure 3. **Inducing CIN by knockdown of CENP-E does not drive tumorigenesis.** (A and B) CENP-E knockdown in the adult thorax (A) and in the wing disc (B). Note the missing bristles in the thorax (arrows). (C) Apoptosis in CENP-E knocked down wing discs. Note that there are more mitotic cells in the dorsal than in the ventral domain. The dotted line separates the dorsal (bottom) from the ventral (top) sides of the wing disc. (D) Mitotic cells on a colchicine-treated wing disc with CENP-E depleted on the dorsal domain. (E) Immunohistochemistry with a CENP-E antibody revealing the CENP-E protein depletion in the dorsal domain of the wing disc. (F and G) Quantification of CENP-E levels in wing discs with CENP-E depleted on the dorsal domain (F) and in wt discs (G). Immunofluorescence intensity was assessed in cells from the dorsal or ventral side independently and shown in a scatter plot with the mean (large horizontal lines) and SD (small horizontal bars). AU, arbitrary unit. (H) Wing disc dissected out of an L3 larvae expressing CENP-E RNAi, p35, and GFP. Note the mild hyperplasia. (I–N) FACS analysis of dissociated ventral (J and M) and dorsal cells (K and N) from wing discs expressing CENP-E RNAi and GFP (I–K) and expressing CENP-E RNAi together with p35 and GFP (L–N). Note the aneuploid cells in K and N. Note that the proportion of GFP versus non-GFP cells is comparable between I (71%/26%) and L (75%/21%), indicating that both compartments grew at a similar rate. The data shown are from a single representative experiment out of three repeats (I–N). (O) Size measurements for discs expressing GFP; GFP and Bub3 RNAi; GFP, Bub3 RNAi, and p35; and GFP, CENP-E, and p35 at the end of the third instar larval stage. For comparison, the percentage of ventral over dorsal (% V/D) volume is also shown. Note that Bub3 RNAi p35 wing discs are larger than the wing discs expressing CENP-E RNAi and p35. (P) Wing discs expressing CENP-E RNAi or CENP-E RNAi with p35 were implanted into adult female hosts to assess their proliferative potential. Error bars represent SD in F, G, and O. Bars: (B–E and I) 40 µm; (H and L) 70 µm.

A

B

C

D

E WT

I NslI RNAi

M NslI RNAi

Q NslI RNAi

U NslI RNAi

F NslI CID

G NslI CID

J NslI CID

K NslI CID

N Bub3 CID

O Bub3 CID

R BubR1 CID

S BubR1 CID

V Mad1 CID

W Mad1 CID

H

	Ventral cells	Dorsal cells
kinetochores without NslI	9%	16%
Total No kinetochores	80	79

L

	Ventral cells	Dorsal cells
kinetochores without NslI	12%	98%
Total No kinetochores	77	72

P

	Ventral cells	Dorsal cells
kinetochores without Bub3	10%	91%
Total No kinetochores	82	81

T

	Ventral cells	Dorsal cells
kinetochores without BubR1	9.7%	98%
Total No kinetochores	72	79

X

	Ventral cells	Dorsal cells
kinetochores without Mad1	8%	98%
Total No kinetochores	75	87

Y

Z

A'

Tumor Growth

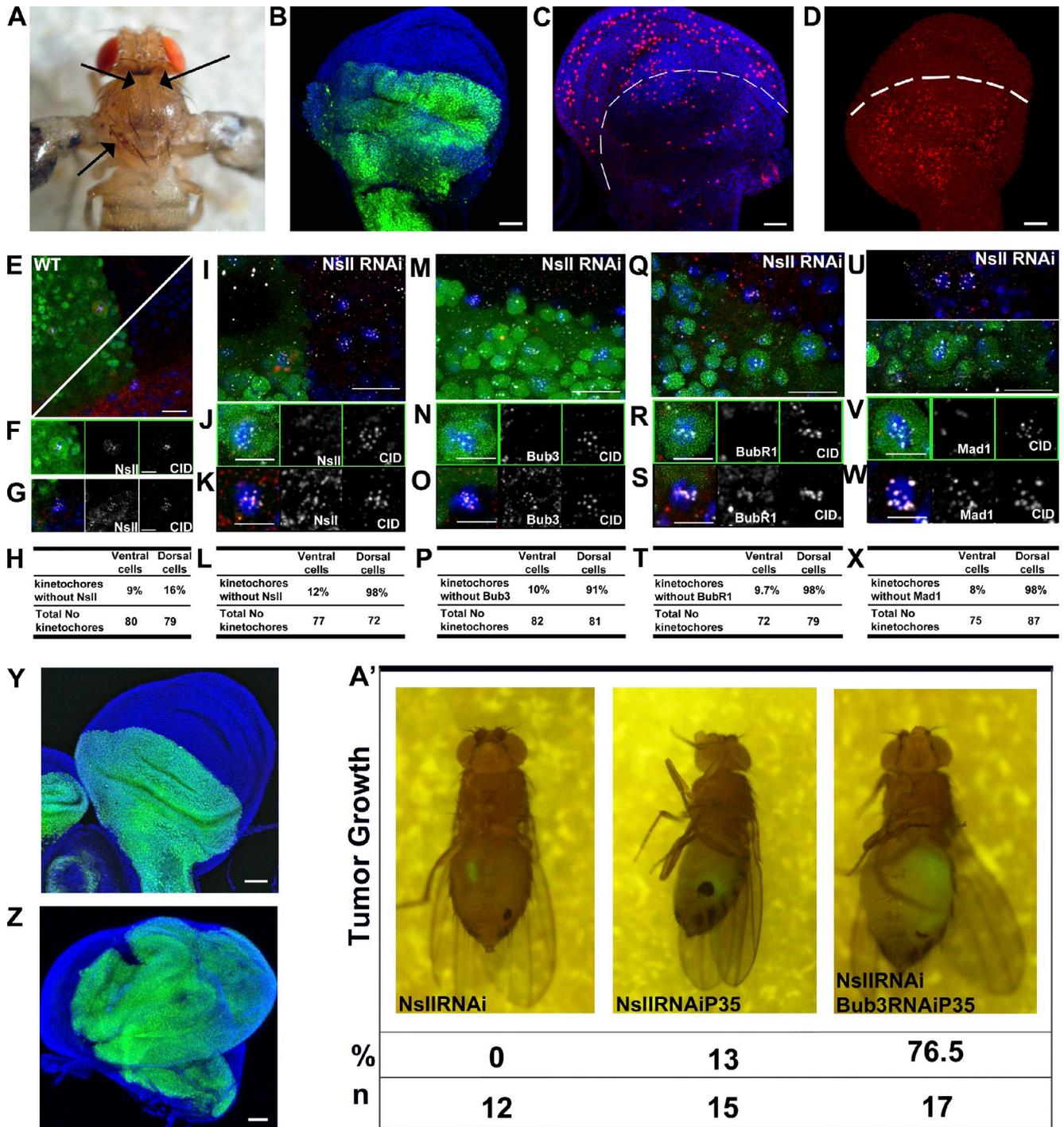|	NsIIRNAi	NsIIRNAiP35	NsIIRNAi Bub3RNAiP35
%	0	13	76.5
n	12	15	17

Figure 4. **Tumorigenesis is not driven by a loss of kinetochore-associated Bub3 but by depletion of the Bub3 cytoplasmic pool.** (A and B) Expression of *nsl1* RNAi in the adult thorax (A) and in the wing imaginal disc (B). Note the lack of bristles in A (arrows) and the morphology of the dorsal compartment of the wing disc (B). (C) Mitotic cells on a colchicine-treated wing imaginal disc with *nsl1* depleted on the dorsal domain. (D) Apoptosis in *nsl1* knocked down wing discs. Note more apoptotic cells in the dorsal than in the ventral domain. In C and D, the dotted lines separate the dorsal (bottom) from the ventral (top) sides of the wing disc. (E–X) SAC components failed to bind kinetochores of cells depleted of *nsl1*. (E–G) wt wing disc. *nsl1* protein in dorsal (F) and ventral cells (G). (I–K, M–O, Q–S, and U–W) Knockdown of *nsl1* in the dorsal compartment. *nsl1* protein in dorsal (F and J) and ventral cells (G and K). (M–O) Bub3 protein in dorsal (N) and ventral cells (O). (Q–S) BubR1 protein in dorsal (R) and ventral cells (S). (U–W) Mad1 protein in dorsal (V) and ventral cells (W). Centromere identifier (CID) labels the centromeres. (H, L, P, T, and X) Quantification of kinetochores analyzed. Note that a high percentage of kinetochores in dorsal cells depleted of *nsl1* failed to show localization of SAC proteins. (Y) Wing disc dissected out of an L3 larvae expressing *nsl1* RNAi, p35, and GFP. Note that this disc is not hyperplastic. (Z) Wing disc simultaneously expressing *nsl1* RNAi, *Bub3* RNAi, p35, and GFP. Note that this disc is hyperplastic. (A') Wing discs expressing *nsl1* RNAi, *nsl1* RNAi and p35, and *nsl1*, *Bub3* RNAi, and p35 were implanted into adult female hosts to assess their proliferative potential. Note that only discs expressing *nsl1*, *Bub3* RNAi, and p35 grew extensively and invaded the host abdomen. Bars: (B–D) 40 µm; (E, I, M, Q, and U) 10 µm; (F, G, J, K, N, O, R, S, V, and W) 5 µm; (Y) 70 µm; (Z) 80 µm.
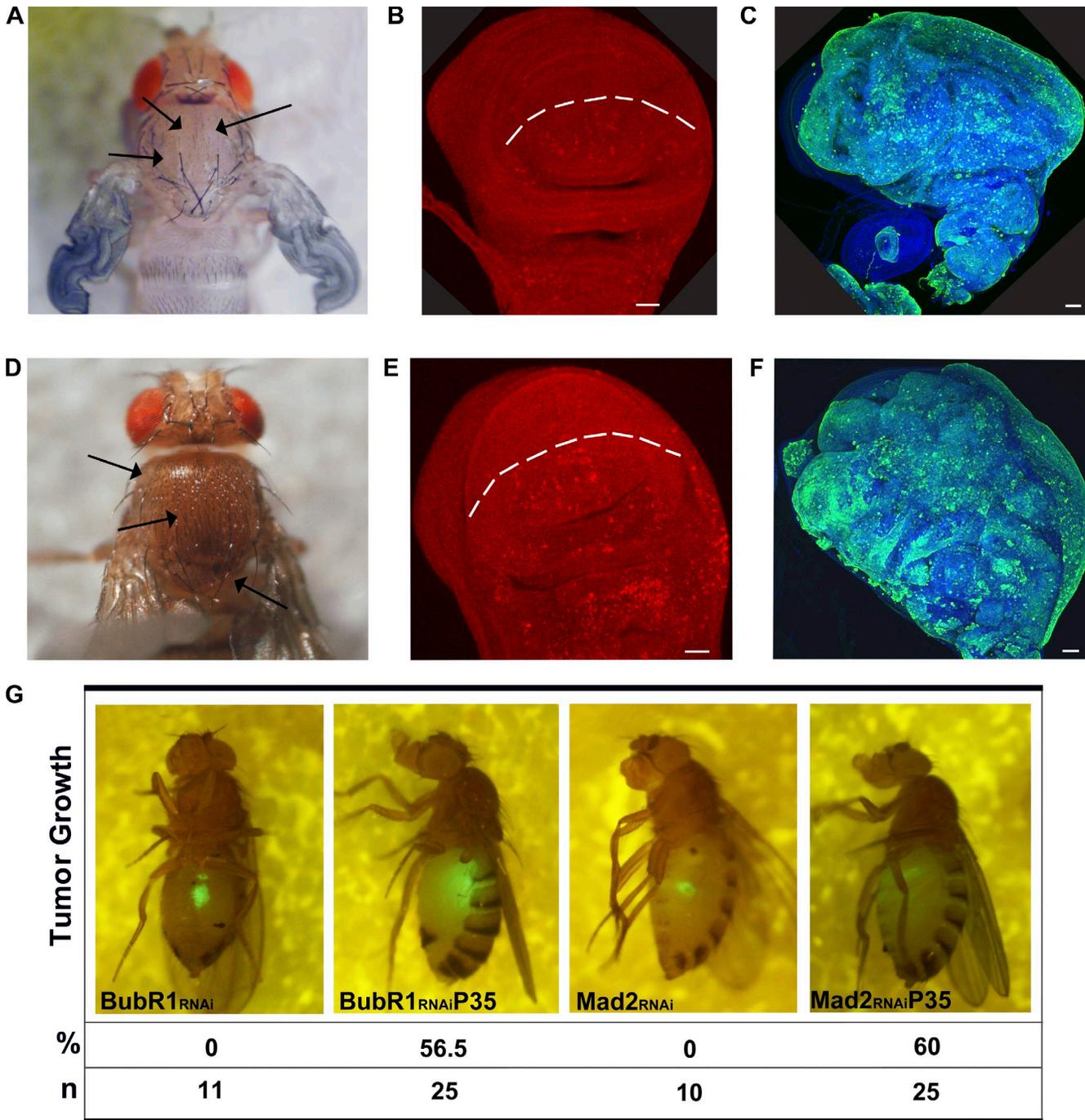
Figure 5. **Knockdown of SAC genes *BubR1* or *Mad2* when apoptosis is inhibited drive tumorigenesis.** (A and D) Knockdown of *BubR1* (A) *Mad2* (D) in the adult thorax. Note the missing bristles (arrows). (B and E) Apoptosis in wing discs expressing *BubR1* RNAi (B) or *Mad2* RNAi (E). Note more apoptosis in the dorsal than in the ventral domain. In B and E, the dotted lines separate the dorsal (bottom) from the ventral (top) sides of the wing disc. (C and F) Wing disc dissected out of an L3 larvae expressing *BubR1* RNAi (C) or *Mad2* RNAi (F) together with p35 and GFP in the dorsal domain of the wing disc. Note the hyperplasia. (G) Hyperplastic wing discs were transplanted into adult female hosts to assess their proliferative potential. Discs expressing GFP and *BubR*1 RNAi; GFP, *BubR1* RNAi, and p35; GFP and *Mad2* RNAi; and GFP, *Mad2* RNAi, and p35 were implanted; the number of implants and the percentage of discs that grew are shown. The implanted *BubR1* RNAi p35– and *Mad2* RNAi p35–expressing discs grew extensively and invaded the host abdomen. Bars: (B and E) 40 µm; (C and F) 80 µm.

transgenic larvae, depletion of BubR1 or Mad2 showed lower frequencies of 30% ($n = 100$ larvae) and 10% ($n = 100$ larvae), respectively. In addition, allograph assays revealed that although *BubR1*– or *Mad2*–knocked down wing discs expressing p35 had the capability to overgrow, these discs demonstrated a less aggressive growth when compared with *Bub3*–knocked down

discs expressing p35 (Fig. 4 G). These results do not appear to be a direct consequence of depletion levels because knockdown levels for *BubR1* and *Mad2* appeared stronger than for *Bub3* (Fig. S1, A–C, E–G, I–K, and N). However, we have not ruled out the effects of *BubR1* and *Mad2* knockdown on *Bub3* levels. Perhaps Bub3 plays an essential role in the tumor suppressor

activity of any SAC protein similar to what has been found for the mitotic checkpoint complex and APC inhibition.

Our data show that checkpoint impairment needs to be associated with failure of apoptosis for tumorigenesis to occur. The mitotic checkpoint is absolutely essential for cellular viability, as knockdown of *Bub3*, *BubR1*, or *Mad2* leads to cell death. The role of blocking apoptosis in causing cancers is known, and it was first realized with the discovery of the Bcl-2 protein, which when combined with a stimulatory oncogene, such as c-myc, could develop cancers very rapidly (Strasser et al., 1990). Another gene well known in human cancers is p53, which also mediates apoptosis and cellular senescence in response to stress (Bieging and Attardi, 2012). However, in our analysis, the apoptosis caused by knocking down *Bub3* did not depend on p53.

In our tumorigenic model, aneuploidy resulting from an impaired SAC is not sufficient to drive tumorigenesis. Previously, it has been reported that aneuploidy generated by mutations in CENP-E in vertebrates may lead to spontaneous tumors with aging (Weaver et al., 2007). In our model, depletion of the CENP-E homologue or other kinetochore proteins that affect microtubule attachment requires depletion of SAC proteins for tumorigenesis to occur. One possibility is that the short period of time during wing development does not allow tumors to develop, and what we are observing is a direct consequence of the action of stimulatory oncogenic growth factors.

The data also show that it is not just SAC signaling provided by the kinetochores that is essential because the absence of Bub3 from the cytosol induces tumorigenesis, suggesting additional roles for the SAC proteins in cycling cells. Other roles for Bub3 have been described, showing it to act as a transcriptional repressor by direct binding to histone deacetylases (Yoon et al., 2004). Histone deacetylases are promising as anticancer drugs owing to their ability to promote apoptosis in a wide range of cancer cells (Warrener et al., 2003). In addition, Bub3 is required during G2 and early stages of mitosis to promote normal mitotic entry. Loss of *Bub3* function by mutation or RNAi depletion causes cells to progress slowly through prophase, a delay that appears to result from a failure in mitotic cyclins A and B accumulation (Lopes et al., 2005). Besides Bub3, other mitotic checkpoint proteins are known to have non-SAC functions: kinetochore–microtubule attachment and nuclear import for Mad1 (Campbell et al., 2001; Emre et al., 2011) and kinetochore–microtubule attachment, cell death, DNA damage response, aging, and megakaryopoiesis for BubR1 (Baker et al., 2004; Wang et al., 2004; Rahmani et al., 2009).

Aneuploidy caused by reduction in one of three essential components of the mitotic checkpoint, Mad2, BubR1 or Bub3, has been implicated (Michel et al., 2001; Babu et al., 2003; Baker et al., 2004) but shown not to be the sole driving force in tumorigenesis (this paper; Castellanos et al., 2008). We propose a new, non-kinetochore-dependent role for these proteins as tumor suppressors. When these checkpoint proteins are present during mitosis, they prevent cells with incorrect chromosomal attachments to the spindle to divide until the error is corrected. They may also control growth by modulating the levels of growth proteins at any given moment during the cell cycle. If Bub3, BubR1, or Mad2 proteins are absent from a cell with an error, this cell will be immediately sent to the apoptotic pathway. If the cell is prevented from dying, all the growth signals that are no longer being modulated by Bub3, BubR1, or Mad2 are now free to act, and the cell undergoes uncontrolled proliferation. Further research is required to find the relationship between apoptosis and Bub3, BubR1, and Mad2 and the growth factors, which are regulated by these proteins.

Materials and methods

Fly strains
The following fly stocks were used: y^1w^{1118} (wt), Ap-Gal4, upstream activation sequence (UAS)-GFP, UAS-*Bub3*^RNAi, UAS-DIAP1, and UAS-p35 (Bloomington *Drosophila* Stock Center) and UAS-*Bub3*^RNAi, UAS-*BubR1*^RNAi, UAS-*Mad2*^RNAi, UAS–CENP-E^RNAi, and UAS-Nsl1^RNAi (obtained from Vienna *Drosophila* RNAi Center; Dietzl et al., 2007).

Antibodies and immunofluorescence
Primary polyclonal antibodies raised against *Drosophila* proteins used were rabbit anti-Bub3 (1:300; Abgent), rabbit anti-BubR1 (1:1,000; Logarinho et al., 2004), rabbit anti-Mad2 (1:10; Logarinho et al., 2004), rabbit anti-Nsl1 (1:200; Venkei et al., 2011), rabbit anti–CENP-E (1:1,000; Wainman et al., 2009), rabbit anti-Mad1 (1:500; unpublished data), and rat anti–centromere identifier (1:1,000; unpublished data). To detect mitotic cells, rabbit antiphospho–histone H3 was used (1:1,000; EMD Millipore). To detect apoptotic cells, rabbit anti–cleaved caspase-3 was used (1:200; Cell Signaling Technology). Secondary antibodies with conjugated fluorescent dyes (Alexa Fluor 488 and Alexa Fluor 568) from the Alexa Fluor series (Invitrogen) were used according to manufacturer's instructions. For immunostaining, wing imaginal discs were fixed in 4% PFA (Sigma-Aldrich) in PBS for 30 min and incubated in blocking solution (0.01% Triton X-100 and 3% BSA in PBS) for 30 min. Imaginal discs were incubated overnight at 4°C in blocking solution with the appropriated primary antibody dilution. Discs were then washed extensively in PBS and incubated for 2 h at room temperature with the secondary antibody diluted in blocking solution. After extensive PBS washes, discs were equilibrated in 50% glycerol with DAPI (Sigma-Aldrich) at 1:200 dilution (stock concentration is 1 mg/ml). Discs were mounted in Vectashield (Vector Laboratories). When required, wing imaginal discs were incubated with 50 µM colchicine for 5 h at 25°C in Schneider's media (Sigma-Aldrich) supplemented with 10% fetal calf serum (Invitrogen) before immunostaining.

Larvae images were acquired with a microscope (SMZ1500; Nikon) equipped with a camera (DS-2M; Nikon). Wing disc images were acquired with a scanning confocal microscope (TCS SP5; Leica) using water immersion 40× (HCX Apochromat L 40×/0.80 NA) and 20× (HCX FL PLAN 20×/0.40 NA) objective lenses. Discs volume (in voxels) was measures with the Volocity software (PerkinElmer). Deconvolution of data stacks was performed with Huygens Essential, version 3.0.2p1 (Scientific Volume Imaging). Fluorescence intensity measurements of total protein for Bub3, Mad2, and CENP-E were performed in 10 regions of interest in a minimum of five wing imaginal discs per genotype using an RGB profiler plugin of ImageJ 1.45h Software (National Institutes of Health). For BubR1 kinetochore depletion measurements, n = 89 for GFP-positive cells, and n = 83 for GFP-negative cells, and for BubR1 in wt kinetochores, n = 79 for GFP-positive cells, and n = 80 for GFP-negative cells. For each cell and each channel, 10 background areas were selected, and the mean background value was subtracted to each individual measured kinetochore. The mitotic index was determined as the ratio of phosphorylated histone H3–positive cells to total cell number, counted in at least five wing imaginal discs per genotype.

Allograft assays
Tissue dissection and injection into adult hosts was performed as previously described (Ashburner, 1989) with minor modifications. A glass Pasteur pipette was pulled to a diameter of 0.5 mm. Third instar larvae, kept at 25°C, were collected 6 d after egg laying. The larvae were washed in PBS, and their wing discs were dissected and transferred into PBS. Before transplantation, young female adult hosts were etherized. One piece of cut wing disc per adult host was injected tangentially in the midventral abdomen. After recovering from anesthesia, the hosts were kept under standard *Drosophila* culture conditions at 25°C. For retransplantation, tumors were dissected, cut in small pieces, and retransplanted into new hosts following the same protocol.

Cytology and flow cytometry
For karyotypes, third instar larvae were dissected in 0.7% NaCl, and their wing imaginal discs were fixed in 0.5% sodium citrate (10 min), 45% acetic

acid (2 min), and 60% acetic acid (1 min). Imaginal discs cells were squashed between a slide and a coverslip and frozen in liquid nitrogen. The coverslip was removed, and the sample was mounted in Vectashield with 1 µg ml^{-1} DAPI (Vector Laboratories). For cellular DNA content analysis, 100 wing imaginal discs of each genotype were dissociated with trypsin-EDTA (Sigma-Aldrich) at 25°C for 2 h with gentle agitation. Dissociated cells were centrifuged at 1,000 rpm for 5 min and fixed with 4% PFA for 15 min. Cells were resuspended in 1.2 ml PBS, and 3 ml of 95% ice-cold ethanol was added dropwise while vortexing. Samples were kept on ice for 30 min before centrifugation at 2,000 rpm for 10 min. The pellet was washed once with PBS and resuspended in PBS with 100 mg/ml RNase (Sigma-Aldrich) and 100 mg/ml propidium iodide (Sigma-Aldrich). Samples were incubated for a further 10 min at RT. For DNA content analysis, we used a flow cytometer (FACSCanto II; BD). Results were analyzed from three independent experiments per genotype using FlowJo (TreeStar, Inc.).

Online supplemental material
Fig. S1 shows the protein depletion levels and the mitotic index in wing imaginal cells. Fig. S2 shows apoptosis in wt wing imaginal discs, discs expressing p35 and imaginal discs from a *Mad2*ᵖ mutant. Online supplemental material is available at http://www.jcb.org/cgi/content/full/jcb.201210018/DC1.

References

Ashburner, M. 1989. Transplantation and in vivo culture. *In Drosophila*: a Laboratory Handbook. Cold Spring Harbor Laboratory Press, Cold Spring Harbor, NY. 243–244.

Babu, J.R., K.B. Jeganathan, D.J. Baker, X. Wu, N. Kang-Decker, and J.M. van Deursen. 2003. Rae1 is an essential mitotic checkpoint regulator that cooperates with Bub3 to prevent chromosome missegregation. *J. Cell Biol.* 160:341–353. http://dx.doi.org/10.1083/jcb.200211048

Baker, D.J., K.B. Jeganathan, J.D. Cameron, M. Thompson, S. Juneja, A. Kopecka, R. Kumar, R.B. Jenkins, P.C. de Groen, P. Roche, and J.M. van Deursen. 2004. BubR1 insufficiency causes early onset of aging-associated phenotypes and infertility in mice. *Nat. Genet.* 36:744–749. http://dx.doi.org/10.1038/ng1382

Bieging, K.T., and L.D. Attardi. 2012. Deconstructing p53 transcriptional networks in tumor suppression. *Trends Cell Biol.* 22:97–106. http://dx.doi.org/10.1016/j.tcb.2011.10.006

Brown, K.D., R.M. Coulson, T.J. Yen, and D.W. Cleveland. 1994. Cyclin-like accumulation and loss of the putative kinetochore motor CENP-E results from coupling continuous synthesis with specific degradation at the end of mitosis. *J. Cell Biol.* 125:1303–1312. http://dx.doi.org/10.1083/jcb.125.6.1303

Buffin, E., D. Emre, and R.E. Karess. 2007. Flies without a spindle checkpoint. *Nat. Cell Biol.* 9:565–572. http://dx.doi.org/10.1038/ncb1570

Campbell, M.S., G.K. Chan, and T.J. Yen. 2001. Mitotic checkpoint proteins HsMAD1 and HsMAD2 are associated with nuclear pore complexes in interphase. *J. Cell Sci.* 114:953–963.

Castellanos, E., P. Dominguez, and C. Gonzalez. 2008. Centrosome dysfunction in *Drosophila* neural stem cells causes tumors that are not due to genome instability. *Curr. Biol.* 18:1209–1214. http://dx.doi.org/10.1016/j.cub.2008.07.029

Cotter, T.G. 2009. Apoptosis and cancer: the genesis of a research field. *Nat. Rev. Cancer.* 9:501–507. http://dx.doi.org/10.1038/nrc2663

Dietzl, G., D. Chen, F. Schnorrer, K.C. Su, Y. Barinova, M. Fellner, B. Gasser, K. Kinsey, S. Oppel, S. Scheiblauer, et al. 2007. A genome-wide transgenic RNAi library for conditional gene inactivation in *Drosophila*. *Nature*. 448:151–156. http://dx.doi.org/10.1038/nature05954

Dobles, M., V. Liberal, M.L. Scott, R. Benezra, and P.K. Sorger. 2000. Chromosome missegregation and apoptosis in mice lacking the mitotic checkpoint protein Mad2. *Cell*. 101:635–645. http://dx.doi.org/10.1016/S0092-8674(00)80875-2

Emre, D., R. Terracol, A. Poncet, Z. Rahmani, and R.E. Karess. 2011. A mitotic role for Mad1 beyond the spindle checkpoint. *J. Cell Sci.* 124:1664–1671. http://dx.doi.org/10.1242/jcs.081216

Hay, B.A., T. Wolff, and G.M. Rubin. 1994. Expression of baculovirus P35 prevents cell death in *Drosophila*. *Development*. 120:2121–2129.

Kalitsis, P., E. Earle, K.J. Fowler, and K.H. Choo. 2000. Bub3 gene disruption in mice reveals essential mitotic spindle checkpoint function during early embryogenesis. *Genes Dev.* 14:2277–2282. http://dx.doi.org/10.1101/gad.827500

Logarinho, E., H. Bousbaa, J.M. Dias, C. Lopes, I. Amorim, A. Antunes-Martins, and C.E. Sunkel. 2004. Different spindle checkpoint proteins monitor microtubule attachment and tension at kinetochores in *Drosophila* cells. *J. Cell Sci.* 117:1757–1771. http://dx.doi.org/10.1242/jcs.01033

Lopes, C.S., P. Sampaio, B. Williams, M. Goldberg, and C.E. Sunkel. 2005. The *Drosophila* Bub3 protein is required for the mitotic checkpoint and for normal accumulation of cyclins during G2 and early stages of mitosis. *J. Cell Sci.* 118:187–198. http://dx.doi.org/10.1242/jcs.01602

Michel, L.S., V. Liberal, A. Chatterjee, R. Kirchwegger, B. Pasche, W. Gerald, M. Dobles, P.K. Sorger, V.V. Murty, and R. Benezra. 2001. MAD2 haplo-insufficiency causes premature anaphase and chromosome instability in mammalian cells. *Nature*. 409:355–359. http://dx.doi.org/10.1038/35053094

Musacchio, A. 2011. Spindle assembly checkpoint: the third decade. *Philos. Trans. R. Soc. Lond. B Biol. Sci.* 366:3595–3604. http://dx.doi.org/10.1098/rstb.2011.0072

Ollmann, M., L.M. Young, C.J. Di Como, F. Karim, M. Belvin, S. Robertson, K. Whittaker, M. Demsky, W.W. Fisher, A. Buchman, et al. 2000. *Drosophila* p53 is a structural and functional homolog of the tumor suppressor p53. *Cell*. 101:91–101. http://dx.doi.org/10.1016/S0092-8674(00)80626-1

Orme, M., and P. Meier. 2009. Inhibitor of apoptosis proteins in *Drosophila*: gatekeepers of death. *Apoptosis*. 14:950–960. http://dx.doi.org/10.1007/s10495-009-0358-2

Pérez-Garijo, A., F.A. Martín, G. Struhl, and G. Morata. 2005. Dpp signaling and the induction of neoplastic tumors by caspase-inhibited apoptotic cells in *Drosophila*. *Proc. Natl. Acad. Sci. USA*. 102:17664–17669. http://dx.doi.org/10.1073/pnas.0508966102

Rahmani, Z., M.E. Gagou, C. Lefebvre, D. Emre, and R.E. Karess. 2009. Separating the spindle, checkpoint, and timer functions of BubR1. *J. Cell Biol.* 187:597–605. http://dx.doi.org/10.1083/jcb.200905026

Strasser, A., A.W. Harris, M.L. Bath, and S. Cory. 1990. Novel primitive lymphoid tumours induced in transgenic mice by cooperation between myc and bcl-2. *Nature*. 348:331–333. http://dx.doi.org/10.1038/348331a0

Sudakin, V., G.K. Chan, and T.J. Yen. 2001. Checkpoint inhibition of the APC/C in HeLa cells is mediated by a complex of BUBR1, BUB3, CDC20, and MAD2. *J. Cell Biol.* 154:925–936. http://dx.doi.org/10.1083/jcb.200102093

Taylor, S.S., E. Ha, and F. McKeon. 1998. The human homologue of Bub3 is required for kinetochore localization of Bub1 and a Mad3/Bub1-related protein kinase. *J. Cell Biol.* 142:1–11. http://dx.doi.org/10.1083/jcb.142.1.1

Venkei, Z., M.R. Przewloka, and D.M. Glover. 2011. *Drosophila* Mis12 complex acts as a single functional unit essential for anaphase chromosome movement and a robust spindle assembly checkpoint. *Genetics*. 187:131–140. http://dx.doi.org/10.1534/genetics.110.119628

Wainman, A., J. Creque, B. Williams, E.V. Williams, S. Bonaccorsi, M. Gatti, and M.L. Goldberg. 2009. Roles of the *Drosophila* NudE protein in kinetochore function and centrosome migration. *J. Cell Sci.* 122:1747–1758. http://dx.doi.org/10.1242/jcs.041798

Wang, Q., T. Liu, Y. Fang, S. Xie, X. Huang, R. Mahmood, G. Ramaswamy, K.M. Sakamoto, Z. Darzynkiewicz, M. Xu, and W. Dai. 2004. BUBR1 deficiency results in abnormal megakaryopoiesis. *Blood*. 103:1278–1285. http://dx.doi.org/10.1182/blood-2003-06-2158

Warrener, R., H. Beamish, A. Burgess, N.J. Waterhouse, N. Giles, D. Fairlie, and B. Gabrielli. 2003. Tumor cell-selective cytotoxicity by targeting cell cycle checkpoints. *FASEB J.* 17:1550–1552.

Weaver, B.A., and D.W. Cleveland. 2006. Does aneuploidy cause cancer? *Curr. Opin. Cell Biol.* 18:658–667. http://dx.doi.org/10.1016/j.ceb.2006.10.002

Weaver, B.A., A.D. Silk, C. Montagna, P. Verdier-Pinard, and D.W. Cleveland. 2007. Aneuploidy acts both oncogenically and as a tumor suppressor. *Cancer Cell.* 11:25–36. http://dx.doi.org/10.1016/j.ccr.2006.12.003

Yoon, Y.M., K.H. Baek, S.J. Jeong, H.J. Shin, G.H. Ha, A.H. Jeon, S.G. Hwang, J.S. Chun, and C.W. Lee. 2004. WD repeat-containing mitotic checkpoint proteins act as transcriptional repressors during interphase. *FEBS Lett.* 575:23–29. http://dx.doi.org/10.1016/j.febslet.2004.07.089